crystals

MDPI

Article

Crystal Structure of an Active Site Mutant Form of IRG1 from *Bacillus subtilis*

Hyun Ho Park

College of Pharmacy, Chung-Ang University, Seoul 06974, Korea; xrayleox@cau.ac.kr

Abstract: Immune-responsive gene1 (IRG1), an enzyme that is overexpressed during immune reactions, catalyzes the production of itaconate from cis-aconitate. Itaconate is a multifunctional immuno-metabolite that displays antibacterial and antiviral activities. The recent resolution of its structure has enabled the mechanism underlying IRG1 function to be speculated on. However, the precise mechanism underlying the enzymatic reaction of IRG1 remains vague owing to the absence of information regarding the structure of the IRG1/substrate or the product complex. In this study, we determined the high-resolution structure of the active site mutant form of IRG1 from *Bacillus subtilis* (bsIRG1_H102A). Structural analysis detected unidentified electron densities around the active site. Structural comparison with the wildtype revealed that H102 was critical for the precise location of the side chain of residues around active site of IRG1. Finally, the activity of bsIRG1 was extremely low compared with that of mammalian IRG1. The current structural study will expectedly help understand the working mechanism of IRG1.

Keywords: crystal structure; immunometabolite; itaconate; immune-responsive gene 1

Citation: Park, H.H. Crystal Structure of an Active Site Mutant Form of IRG1 from *Bacillus subtilis*. *Crystals* **2021**, *11*, 350. https://doi.org/10.3390/cryst11040350

Academic Editor: Kyeong Kyu Kim

Received: 11 March 2021
Accepted: 26 March 2021
Published: 29 March 2021

1. Introduction

Itaconate is an unsaturated dicarboxylic acid, which functions as an intermediate metabolite in the tricarboxylic acid (TCA) cycle [1]. Owing to the wide usage of itaconate in industrial applications, such as the production of various resins and bioactive compounds, itaconate has become the subject of intensive material science-based research [2,3]. However, in biology, itaconate is known for the role it plays in regulating innate immunity as well as for its antibacterial and antiviral activities [4–6]. Antimicrobial activity of itaconate was initially reported in fungi [7]. *Aspergillus terreus*, a representative fungus, produces high levels of itaconate that act against *Pseudomonas indigofera* and *Mycobacterium tuberculosis* by directly inhibiting the activity of housekeeping enzymes, such as isocitrate lyase (ICL) and fructose-6-phosphate 2-kinase [8–10]. The antimicrobial activity of itaconate in the mammalian system has also been revealed recently [4–6]. Itaconate eliminates infections caused by bacteria, such as *Salmonella enterica* and *M. tuberculosis*, by targeting ICL [4]. Itaconate reportedly inhibits succinate dehydrogenase activity during Zika virus infections [5].

Immune responsive gene 1 (IRG1), also known as cis-aconitate decarboxylase (CAD), is a ~55 kDa enzyme that catalyzes the decarboxylation of cis-aconitate to generate itaconate [11,12]. Recent mammalian system studies indicate that IRG1, which is overexpressed in macrophages in response to pathogen-associated molecular patterns (PAMPs) such as lipopolysaccharides (LPS), catalyzes the overproduction of itaconate against pathogenic infections [4,13–15]. Since excessive production of itaconate caused by abnormal overexpression of IRG1 induces gout [16], chronic arthritis [17], and tumor progression in mouse models [18], targeting IRG1 may lead to therapeutic intervention in various human diseases.

Due to increased interest in the role of itaconate as well as its production, the mechanism underlying IRG1-mediated itaconate production, using cis-aconitate as a substrate,

is being intensively researched biochemically as well as structurally [19–21]. Structural studies of mammalian IRG1 have helped determine the dynamic open-closed structure of IRG1 as well as its putative active site [19,20], while the results of structural studies conducted on IRG1 from *B. subtilis* have led to a tentative functional mechanism being proposed for IRG1 [21]. Despite recent structural and enzymatic studies, the precise catalytic mechanism of IRG1 in the innate immunity process has remained elusive. In this study, we resolved the high-resolution structure of active site mutant form of IRG1 from *B. subtilis* (bsIRG1_H102A). Comparative structural analyses, accompanied by an enzymatic activity assay, were used to determine features of bsIRG1_H102A. Our current investigation of the active site mutant form of bsIRG1 may provide helpful information regarding the substrate binding process of IRG1 and the functional mechanism underlying this process.

2. Materials and Methods

2.1. Site-Directed Mutagenesis

A quickchange mutagenesis kit (Stratagene) was used for site-directed mutagenesis. The expression plasmid containing a full-length *IRG1* gene from *B. subtilis* (corresponding to amino acids 1–445) was used for the template. Induced mutagenesis of H102A was then confirmed via sequencing.

2.2. Protein Expression and Purification

The plasmid encoding bsIRG1_H102A was transformed into *Escherichia coli* BL21 (DE3) cells. A single colony was picked and cultured in 5 mL lysogeny broth (LB) medium containing 50 μg/mL kanamycin overnight at 37 °C. Cells from the small culture were then transferred and cultured in 1 L of medium until optical density (OD) of approximately 0.65 was reached at 600 nm, at which point 0.3 mM isopropyl β-D-1-thiogalactopyranoside (IPTG) was added to the medium. Next, the cells were further cultured for 22 h at 20 °C. Cells, collected after harvesting via centrifugation at 20 °C, were suspended with 40 mL of lysis buffer (20 mM Tris-HCl [pH 8.0], 500 mM NaCl, and 25 mM imidazole) containing a serine protease inhibitor (phenylmethanesulfonyl fluoride; Sigma-Aldrich, St. Louis, MO, USA). After the cells were lysed via sonication, cell debris was removed by centrifugation at 10,000× g for 30 min at 4 °C. Then, the supernatant was collected and mixed with nickel nitrilotriacetic acid (Ni-NTA) resin (Qiagen, Hilden, Germany) using gentle agitation, for 4 h at 4 °C. The resulting mixture was applied to a gravity-flow column and washed with 50 mL of washing buffer (20 mM Tris-HCl [pH 8.0], 500 mM NaCl, and 60 mM imidazole). Next, a total of 2 mL of elution buffer (20 mM Tris-HCl [pH 7.9], 500 mM NaCl, and 250 mM imidazole) was applied to the column to elute the bound target protein. The eluted target protein was concentrated to 30 mg/mL and sequentially subjected to size-exclusion chromatography, which was conducted via an ÄKTA explorer system (GE Healthcare, Chicago, IL, USA) equipped with a Superdex 200 Increase 10/300 GL 24 mL column (GE Healthcare) pre-equilibrated with SEC buffer (20 mM Tris-HCl [pH 8.0] and 150 mM NaCl). Peak fractions were pooled, concentrated to 8.5 mg/mL, flash-frozen in liquid N_2, and stored at −80°C until further use. Mouse and human IRG1 proteins, used for the activity study, were prepared using the same method used to purify bsIRG1 protein [21]. The accession numbers (NCBI reference sequences) for the sequence of bsIRG1, mouseIRG1, and humanIRG1 are ARW33836, NP_032418, and NP_001245335, respectively.

2.3. Crystallization and Data Collection

Crystallization of bsIRG1_H102A was conducted via the same method used for wild-type bsIRG1, and crystals were obtained under conditions that were similar to those used to produce wildtype crystals [20]. Briefly, 1 μL of protein solution was mixed with an equal volume of reservoir solution containing 1.4 M ammonium sulfate, 0.1 M CAPS pH 10.2, and 0.2 M lithium sulfate and the droplets were allowed to equilibrate against 300 μL of mother liquor using the hanging drop vapor diffusion method at 20 °C. For purpose of data collection, crystals were soaked in a cryoprotectant solution consisting of mother liquor

supplemented with 40% (v/v) glycerol. These crystals were flash-cooled in a N_2 stream at −178 °C. X-ray diffraction data were collected at the Pohang Accelerator Laboratory with the 5C beamline (Pohang, Republic of Korea). The diffraction data were indexed, integrated, and scaled using the HKL-2000 program [22].

2.4. Structure Determination and Analysis

The molecular replacement (MR) phasing method was used for initial phasing determination. A PHASER [23] in PHENIX package was employed for MR. The previously solved wild-type structure of bsIRG1 (PDB ID: 7BRA) was used as the search model [20]. The initial model was built automatically with AutoBuild in PHENIX [24]. Further model building and refinement were performed using Coot [25] and Phenix.refine in PHENIX package [24]. Model quality was validated using MolProbity [26]. All structural figures were produced via the PyMOL program [27].

2.5. Decarboxylation Activity Test and HPLC Analysis

To conduct enzymatic activity tests, a final 100 µL reaction solution was prepared in 25 µM HEPES buffer pH 7.1 supplied with 0.5 µM of each IRG1 enzyme and 1.5 mM cis-aconitate as substrate. The reaction, which proceeded for 1 h at 30°C, was stopped by adding 400 µL methanol [28]. Next, the reaction mixture was analyzed using Agilent High-Pressure Liquid Chromatography (HPLC) equipped with an ACC-3000 autosampler, Mightysil RP-18 GP reverse-phase C18 column (150 V, 4.6 mm, Japan) and a DAD-3000 diode array detector. The mobile phase consisted of water mixed with 0.1% trifluoroacetic acid as solution A and HPLC-grade acetonitrile as solution B. Substrates and their products were detected via a UV detector at 210 nm. All HPLC experiments were performed at 30°C. The flow rate used to separate the sample was set to 0.9 mL/min, and solution A was maintained at 95% for 40 min for analysis.

2.6. Structural Data Accession Number

Coordinate and structural factors were deposited with the Protein Data Bank under PDB ID: 7E9D.

3. Results

3.1. Preliminary X-ray Crystallographic Studies of bsIRG1_H102A

IRG1 converts cis-aconitate to itaconate, an important immuno-metabolite that acts against pathogens (Figure 1a). Previous structural and enzymatic studies have indicated that seven residues are present around the active site. These residues, namely D93 (D91 in bsIRG1), T97 (T95 in bsIRG1), H103 (H102 in bsIRG1), H159 (H151 in bsIRG1), K207 (K200 in bsIRG1), K272 (K266 in bsIRG1), and Y318 (A310 in bsIRG1), play a critical role in mammalian IRG1 activity [19,20]. To understand the precise enzymatic mechanism of bsIRG1, together with the function of H102, we attempted to characterize and solve the structure of bsIRG1_H102A.

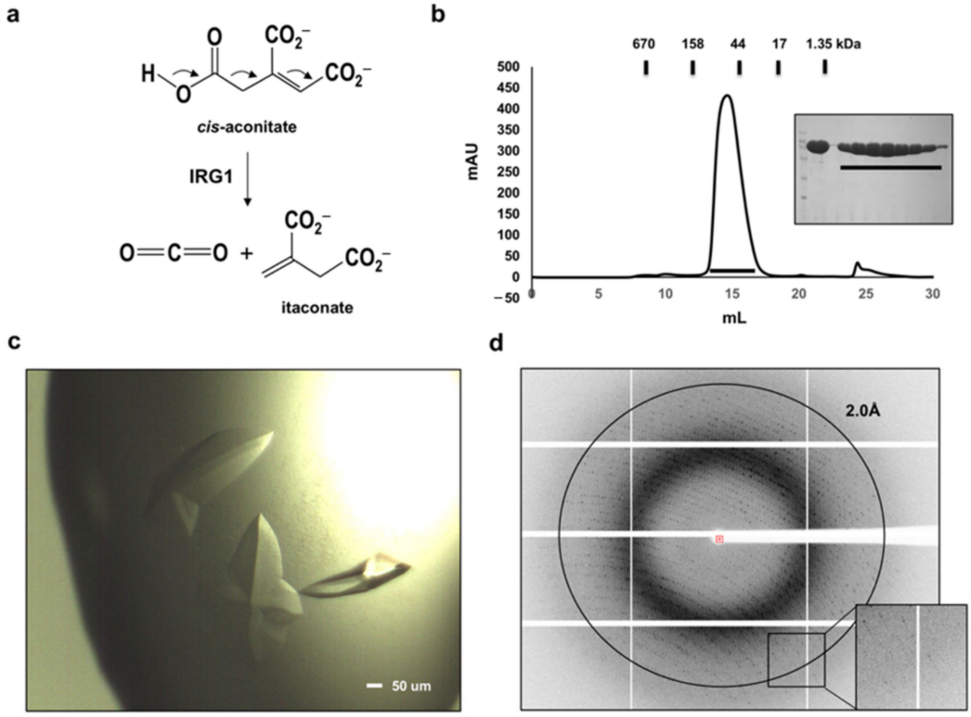

Figure 1. Crystallization and X-ray crystallographic studies of bsIRG1_H102A. (**a**) Schematic of the enzymatic reaction of IRG1 that produce itaconate using cis-aconitate as a substrate. (**b**) Profile of FPLC used for purification of bsIRG1_H102A. SDS-PAGE was provided at the right side of peak. Black bar indicates the fractions from FPLC loaded onto SDS-PAGE. The position of size standard markers is also provided above the FPLC profile. (**c**) The crystal of bsIRG1_H102A. A scale bar is shown at the bottom right-hand corner of the crystal image. (**d**) Diffraction image. Diffraction spots around 2.0 Å were magnified.

In preparation for structural and biochemical studies, the active site mutant form of bsIRG1 (bsIRG1_H102A) was purified via a quick two step chromatographic procedure. His-tag affinity chromatography followed by size-exclusion chromatography produced a ~95% pure bsIRG1_H102A protein with no contaminating bands, as was observed upon analysis via SDS-PAGE (Figure 1b). The monomeric molecular weight of bsIRG1_H102A including the N-terminal His-tag was estimated to be 47.5 kDa, and its size-exclusion chromatography elution peak suggested that, similar to the wildtype, it exists as a dimer in solution, (Figure 1b). This indicated that introducing the mutant to alanine at H102 did not affect the stoichiometry of bsIRG1 in solution.

The purified protein was crystallized in one day and the crystals were grown to a maximum size of 0.5 × 0.1 × 0.1 mm^3 (Figure 1c). The crystals were diffracted to 1.89 Å at the synchrotron (Figure 1d). The crystals belonged to space group $P2_12_12_1$ with unit-cell parameters of a = 58.91, b = 110.77, c = 168.56 Å. Diffraction statistics are shown (Table 1).

Table 1. Crystallographic statistics.

Data Collection	**bsIRG1_H102A**
X-ray source	Synchrotron (PAL 5C)
Detector	Eiger 9M
Wavelength	0.97950
Space group	$P2_12_12_1$
Cell dimensions	
a, b, c	58.91 Å, 110.77 Å, 168.56 Å
α, β, γ	90°, 90°, 90°
† Resolution	50.00–1.89 (1.93–1.89) Å
Wilson B-factor	21.38 Å^2
† No. of unique reflections overall	85,234 (5,322)
† Rsym	0.064 (0.754)
† I/σI	18.7 (2.1)
† Completeness	95.6% (91.3%)
† Redundancy	9.8 (8.9)
CC1/2	0.99 (0.79)
Refinement	
† Resolution	40.35–1.89 (1.91–1.89) Å
No. of reflections used (completeness)	85,146 (95.5%)
No. of non-H protein atoms	6,688
No. of water molecules	763
No. of ions	0
† Rwork	17.21% (24.24%)
† Rfree	20.21% (26.57%)
Average B-factors	
Protein	22.9 Å^2
Water molecules	34.4 Å^2
r.m.s. deviations	
Bond lengths	0.006 Å
Bond angles	0.774°
Ramachandran Plot	
Ramachandran outliers	0.00%
Ramachandran favored	99.32%
Ramachandran allowed	0.68%
Rotamer outliers	0.00%
Clash score	2.25

† The highest resolution shell is presented in parenthesis. r.m.s, root mean square.

3.2. Overall Structure of H102A Mutant Form of bsIRG1

The structure of bsIRG1_H102A was solved using the molecular replacement phasing method with wildtype structure as the search model. The structure was refined to R_{work} = 17.21% and R_{free} = 20.21%. The refinement statistics are summarized in Table 1. The asymmetric unit comprised two molecules, with the final model encompassing residues 5–445 for both molecules (Figure 2a). The structures of the two molecules in the asymmetric unit were nearly identical, with a root mean square deviation (RMSD) of 0.46 Å. Phylogenetic analysis of homologous IRG1 sequences from various species using the ConSurf server [29] indicated that the residues involved in the formation of the putative active site, including H102, were highly conserved as expected (Figure 2b).

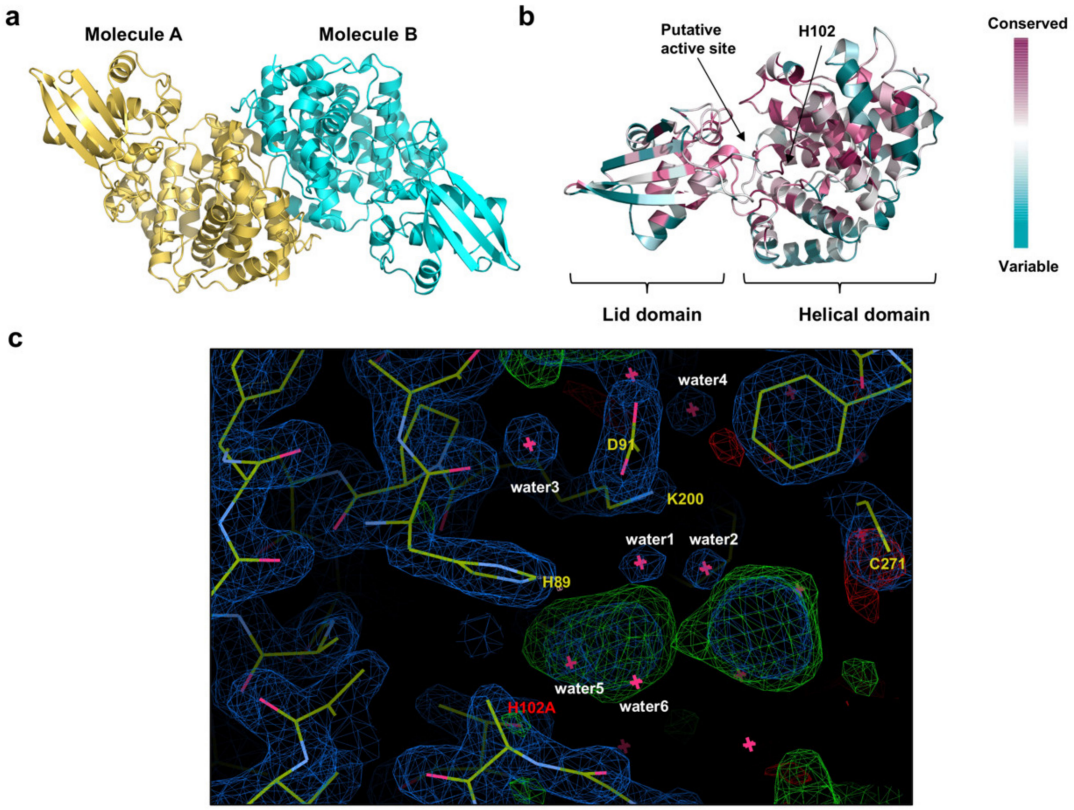

Figure 2. Structure of bsIRG1_H102A and the active site around H102. (**a**) Crystal structure of bsIRG1_H102A. Two molecules in an asymmetric unit, molecules A and B, are presented via a cartoon model. (**b**) Cartoon representation of bsIRG1 with colors indicating the degree of amino acid sequence conservation, as analyzed by Consurf. Two distinct IRG1 domains, the lid and helical domains, are indicated. The positions of the putative active site and H102 site are indicated by black arrows (**c**) 2fo-fc map (blue mesh) and fo-fc map (green mesh) contoured at the 1-σ level for 2fofc map and 2.5-σ level around the mutated residue, H102A.

The first structural analysis that was performed using this high-resolution structure led to the identification of the mutation site, H102. Absolute absence of the electron density corresponding to the histidine side chain at the H102 site indicated that the H102 residue had successfully mutated to alanine via mutagenesis (Figure 2c). Because the H102 residue in the putative active site of IRG1 is one of the residues critical for IRG1 activity, our structural analysis of bsIRG1_H102A focused on the region around the H102 site, where we observed two large unidentified bulb-like densities, which had a much higher density than that of water but were not structurally fit to accommodate either the substrate or product (Figure 2c).

3.3. Comparison of the Structure of bsIRG1_H102A with the Structure of Wildtype bsIRG1

Structural comparison between the wildtype and mutant via superimposition analysis indicated that the structures were nearly identical, exhibiting a RMSD of 0.483 Å and TM-score of 0.923 (Figure 3a). Despite such structural similarities, structural comparison between bsIRG1_H102A and the wildtype, with particular reference to the putative active site around the H102 residue, revealed that the location of the side chains of several residues, including those of H89, R100, and K200, were altered due to H102A mutagenesis (Figure 3b). Loss of the bulky side chain of histidine due to mutagenesis allowed the ring structure of H89 to rotate causing the location of the side chain of K200 to move slightly (Figure 3b). The most dramatic change in the structure of the side chain was detected at the R100 residue. The temperature factors of residue R100 in the wildtype and mutant protein

are 32 Å^2 and 35 Å^2, respectively. Introduction of the mutation caused the side chain of this residue to locate away from H102 (Figure 3b).

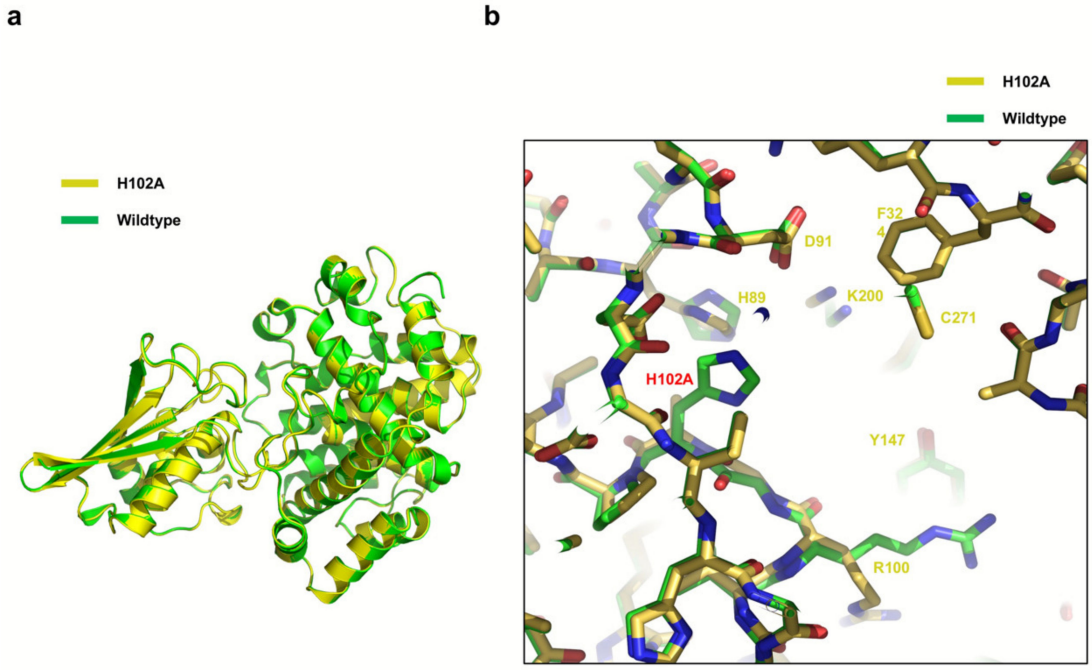

Figure 3. Structural comparison of bsIRG1_H102A with wildtype bsIRG1: (**a**) superimposition of bsIRG1_H102A (yellow color) on wildtype bsIRG1 (green color); and (**b**) magnified view of the active site around the H102 residue.

3.4. Activity Comparison of bsIRG1 with Mammalian IRG1

To confirm the functional importance of the H102 residue in bsIRG1 (H103 residue in mammalian IRG1), the activities of both wildtype bsIRG1 and bsIRG1_H102A were tested using high-pressure liquid chromatography (HPLC). Before the activity test, the standard elution positions of cis-aconitate and itaconate were determined via HPLC (Figure 4a,b). For the enzymatic activity test, the reaction mixture, including cis-aconitate and wildtype bsIRG1 or bsIRG1_H102A, was loaded onto the HPLC apparatus, following which itaconate production was monitored by analyzing the eluted position of the newly produced compound. The HPLC profile showed that only a minute amount of itaconate was produced by wildtype bsIRG1 (Figure 4c), whereas no itaconate at all was produced by the bsIRG1_H102A mutant (Figure 4d). Because the activity of bsIRG1 in this experiment was seen to be low, we compared the activity of bsIRG1 with mammalian IRG1 (IRG1 from mouse and human). This experiment showed that similar amounts of itaconate (although a much larger amount when compared with the peak corresponding to wildtype bsIRG1), were produced by both mouse IRG1 and human IRG (Figure 4e,f), indicating that mammalian IRG1 displayed stronger cis-aconitate decarboxylase activity compared with that of bsIRG1.

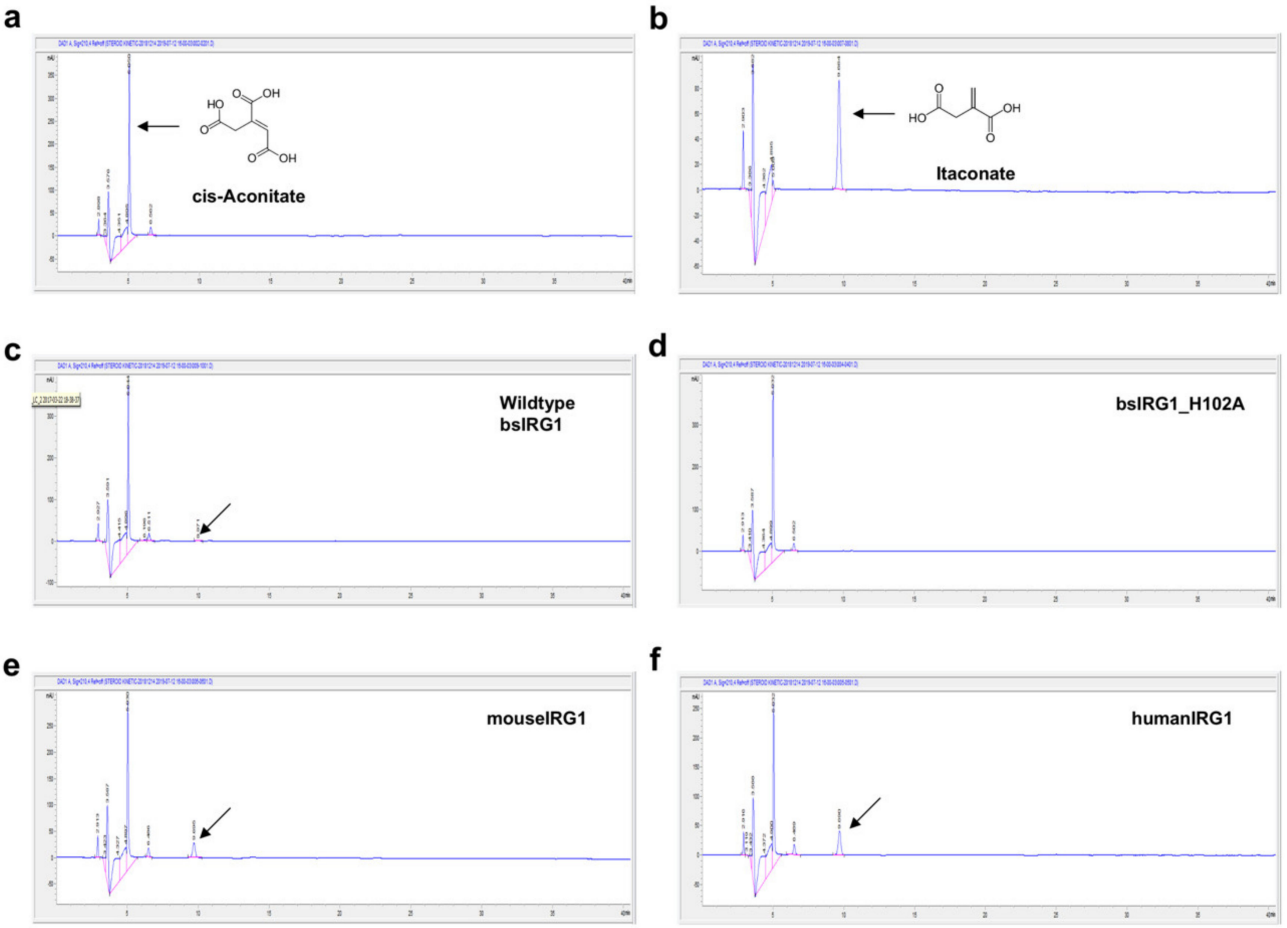

Figure 4. Comparative analysis of bsIRG1 and mammalian IRG1 activities. (**a**,**b**) HPLC profiles. The eluted standard positions of cis-aconitate (**a**) and itaconate (**b**) are indicated by black arrows. (**c**) HPLC profile showing wildtype bsIRG1 activity. The peak produced by the enzymatic reaction is indicated by a black arrow. (**d**) HPLC profile showing bsIRG1_H102A activity. No peak was observed for itaconate. (**e**,**f**) HPLC profiles showing the activities of mouseIRG1 and humanIRG1. The peaks produced by the enzymatic reaction are indicated by a black arrow.

4. Discussion

To understand the precise mechanism by which IRG1 catalyzes the production of itaconate during microbial infection, we solved the structure of the active site mutant variant of IRG1 found in *B. subtilis* (bsIRG1_H102A). We investigated the manner in which the structure of this variant H102 residue, critical for IRG1 activity, is mutated to alanine. Previous structural and modeling studies have suggested that H102 may be the key residue, because it provides a general base for electron transfer during the decarboxylation process [20].

Biochemical analysis of bsIRG1_H102A variant showed that H102A mutation did not affect the formation of a functional IRG1 dimer, while phylogenic sequence analysis indicated that residues around the putative active site, including H102, were well conserved throughout different species (Figure 2b). During the structural analysis of bsIRG1_H102A, we found two bulb-like electron densities around the active site (near H102) (Figure 2c). These densities, which were much larger than that of water, did not fit either the substrate or the product. Because we did not add any substrate or product during structural determination, these densities may have been produced by ions or unidentified molecules that are present in cells used for protein expression. Since these unidentified densities were located within the pocket of the putative active site, further investigations may be required to identify these densities.

Although the overall structure of the bsIRG1_H102A variant is almost identical with that of wildtype bsIRG1, structure comparison by superimposition analysis indicated that the location of the side chains of H89, R100, and K200, which are critical for the activity of IRG1, were altered by introduction of the mutation. For example, the histidine ring of H89 rotated 90° and the location of the side chain of K200 was slightly moved. In the case of R100, the side chain was kinked to 90° and localized far away from the active site. This observation indicated that H102 may be crucial for accurate formation of the active site, which is critical for the proper activity of IRG1, although H102 has been suggested as one of the key general bases that can transfer electron during the decarboxylation reaction [20].

Interestingly, activity analysis of bsIRG1 indicated that it exhibits extremely low activity compared with mammalian IRG1. Such low bsIRG1 activity may be explained by the failure to find specific reaction conditions. Beside this, our previous finding, which showed that the active site of bsIRG1 was highly similar to the active site of IDS epimerase, may explain the limited nature of bsIRG1 activity [20]. H99 and Y145 in the active site of IDS epimerase are known to be critical for the epimerization reaction [30]. During the previous study, we observed that these two residues were conserved only in bsIRG1, and not in mammalian IRG1 [20]. In addition to this similarity between bsIRG1 and epimerase, differences between the active sites of bsIRG1 and mammalian IRG1 have been also observed. Two residues, H277 and Y318 in human IRG1 (Y319 in mouse IRG1), which were previously identified as critical for IRG1 activity [19], are not conserved in bsIRG1. This structural analysis showed that the active site composition of bsIRG1 is more similar to that of epimerase than to that of mammalian IRG1. Further activity analysis of bsIRG1 may have to be performed to elucidate the unknown causes leading to low IRG1 activity and the relationship between decarboxylase activity and epimerase activity of bsIRG1.

Funding: This study was supported by the National Research Foundation (NRF) of Korea, which is funded by the Ministry of Science, ICT (Information and Communication Technology), and Future Planning (MSIP) (2017M3A9D8062960 and 2018R1A4A1023822) of the Korean Government.

Data Availability Statement: Not applicable.

Acknowledgments: The author thanks members of the Park laboratory for helpful discussions.

Conflicts of Interest: The author declares no conflict of interest.

References

1. O'Neill, L.A.J.; Artyomov, M.N. Itaconate: The poster child of metabolic reprogramming in macrophage function. *Nat. Rev. Immunol.* **2019**, *19*, 273–281. [CrossRef] [PubMed]
2. Kurian, J.V. A new polymer platform for the future—Sorona (R) from corn derived 1,3-propanediol. *J. Polym. Environ.* **2005**, *13*, 159–167. [CrossRef]
3. Cordes, T.; Michelucci, A.; Hiller, K. Itaconic Acid: The Surprising Role of an Industrial Compound as a Mammalian Antimicrobial Metabolite. *Annu. Rev. Nutr.* **2015**, *35*, 451–473. [CrossRef]
4. Michelucci, A.; Cordes, T.; Ghelfi, J.; Pailot, A.; Reiling, N.; Goldmann, O.; Binz, T.; Wegner, A.; Tallam, A.; Rausell, A.; et al. Immune-responsive gene 1 protein links metabolism to immunity by catalyzing itaconic acid production. *Proc. Natl. Acad. Sci. USA* **2013**, *110*, 7820–7825. [CrossRef]
5. Daniels, B.P.; Kofman, S.B.; Smith, J.R.; Norris, G.T.; Snyder, A.G.; Kolb, J.P.; Gao, X.; Locasale, J.W.; Martinez, J.; Gale, M.; et al. The Nucleotide Sensor ZBP1 and Kinase RIPK3 Induce the Enzyme IRG1 to Promote an Antiviral Metabolic State in Neurons. *Immunity* **2019**, *50*, 64–76.e4. [CrossRef]
6. Nair, S.; Huynh, J.P.; Lampropoulou, V.; Loginicheva, E.; Esaulova, E.; Gounder, A.P.; Boon, A.C.M.; Schwarzkopf, E.A.; Bradstreet, T.R.; Edelson, B.T.; et al. Irg1 expression in myeloid cells prevents immunopathology during M-tuberculosis infection. *J. Exp. Med.* **2018**, *215*, 1035–1045. [CrossRef]
7. Bentley, R.; Thiessen, C.P. Biosynthesis of itaconic acid in Aspergillus terreus. III. The properties and reaction mechanism of cis-aconitic acid decarboxylase. *J. Biol. Chem.* **1957**, *226*, 703–720. [CrossRef]
8. Khan, F.R.; Mcfadden, B.A. Enzyme Profiles in Seedling Development and the Effect of Itaconate, an Isocitrate Lyase-Directed Reagent. *Plant Physiol.* **1979**, *64*, 228–231. [CrossRef] [PubMed]
9. Sakai, A.; Kusumoto, A.; Kiso, Y.; Furuya, E. Itaconate reduces visceral fat by inhibiting fructose 2,6-bisphosphate synthesis in rat liver. *Nutrition* **2004**, *20*, 997–1002. [CrossRef]

10. Li, A.; Pfelzer, N.; Zuijderwijk, R.; Punt, P. Enhanced itaconic acid production in Aspergillus niger using genetic modification and medium optimization. *BMC. Biotechnol.* **2012**, *12*, 57. [CrossRef] [PubMed]
11. Dwiarti, L.; Yamane, K.; Yamatani, H.; Kahar, P.; Okabe, M. Purification and characterization of cis-aconitic acid decarboxylase from Aspergillus terreus TN484-M1. *J. Biosci. Bioeng.* **2002**, *94*, 29–33. [CrossRef]
12. Kanamasa, S.; Dwiarti, L.; Okabe, M.; Park, E.Y. Cloning and functional characterization of the cis-aconitic acid decarboxylase (CAD) gene from Aspergillus terreus. *Appl. Microbiol. Biot.* **2008**, *80*, 223–229. [CrossRef] [PubMed]
13. Mills, E.L.; Ryan, D.G.; Prag, H.A.; Dikovskaya, D.; Menon, D.; Zaslona, Z.; Jedrychowski, M.P.; Costa, A.S.H.; Higgins, M.; Hams, E.; et al. Itaconate is an anti-inflammatory metabolite that activates Nrf2 via alkylation of KEAP1. *Nature* **2018**, *556*, 113–117. [CrossRef]
14. Basler, T.; Jeckstadt, S.; Valentin-Weigand, P.; Goethe, R. Mycobacterium paratuberculosis, Mycobacterium smegmatis, and lipopolysaccharide induce different transcriptional and post-transcriptional regulation of the IRG1 gene in murine macrophages. *J. Leukoc. Biol.* **2006**, *79*, 628–638. [CrossRef]
15. Strelko, C.L.; Lu, W.Y.; Dufort, F.J.; Seyfried, T.N.; Chiles, T.C.; Rabinowitz, J.D.; Roberts, M.F. Itaconic Acid Is a Mammalian Metabolite Induced during Macrophage Activation. *J. Am. Chem. Soc.* **2011**, *133*, 16386–16389. [CrossRef]
16. Pessler, F.; Mayer, C.T.; Jung, S.M.; Behrens, E.M.; Dai, L.; Menetski, J.P.; Schumacher, H.R. Identification of novel monosodium urate crystal regulated mRNAs by transcript profiling of dissected murine air pouch membranes. *Arthritis Res. Ther.* **2008**, *10*, R64. [CrossRef] [PubMed]
17. Michopoulos, F.; Karagianni, N.; Whalley, N.M.; Firth, M.A.; Nikolaou, C.; Wilson, I.D.; Critchlow, S.E.; Kollias, G.; Theodoridis, G.A. Targeted Metabolic Profiling of the Tg197 Mouse Model Reveals Itaconic Acid as a Marker of Rheumatoid Arthritis. *J. Proteome Res.* **2016**, *15*, 4579–4590. [CrossRef] [PubMed]
18. Weiss, J.M.; Davies, L.C.; Karwan, M.; Ileva, L.; Ozaki, M.K.; Cheng, R.Y.; Ridnour, L.A.; Annunziata, C.M.; Wink, D.A.; McVicar, D.W. Itaconic acid mediates crosstalk between macrophage metabolism and peritoneal tumors. *J. Clin. Investig.* **2018**, *128*, 3794–3805. [CrossRef]
19. Chen, F.F.; Lukat, P.; Iqbal, A.A.; Saile, K.; Kaever, V.; van den Heuvel, J.; Blankenfeldt, W.; Bussow, K.; Pessler, F. Crystal structure of cis-aconitate decarboxylase reveals the impact of naturally occurring human mutations on itaconate synthesis. *Proc. Natl. Acad. Sci. USA* **2019**, *116*, 20644–20654. [CrossRef]
20. Chun, H.L.; Lee, S.Y.; Lee, S.H.; Lee, C.S.; Park, H.H. Enzymatic reaction mechanism of cis-aconitate decarboxylase based on the crystal structure of IRG1 from Bacillus subtilis. *Sci. Rep.* **2020**, *10*, 11305. [CrossRef] [PubMed]
21. Chun, H.L.; Lee, S.Y.; Kim, K.H.; Lee, C.S.; Oh, T.J.; Park, H.H. The crystal structure of mouse IRG1 suggests that cis-aconitate decarboxylase has an open and closed conformation. *PLoS ONE* **2020**, *15*, e0242383. [CrossRef]
22. Otwinowski, Z.; Minor, W. Processing of X-ray diffraction data collected in oscillation mode. *Methods Enzymol.* **1997**, *276*, 307–326. [PubMed]
23. McCoy, A.J. Solving structures of protein complexes by molecular replacement with Phaser. *Acta Crystallogr. D Biol. Crystallogr.* **2007**, *63*, 32–41. [CrossRef] [PubMed]
24. Adams, P.D.; Afonine, P.V.; Bunkoczi, G.; Chen, V.B.; Davis, I.W.; Echols, N.; Headd, J.J.; Hung, L.W.; Kapral, G.J.; Grosse-Kunstleve, R.W.; et al. PHENIX: A comprehensive Python-based system for macromolecular structure solution. *Acta Crystallogr. D Biol. Crystallogr.* **2010**, *66*, 213–221. [CrossRef]
25. Emsley, P.; Cowtan, K. Coot: Model-building tools for molecular graphics. *Acta Crystallogr. D Biol. Crystallogr.* **2004**, *60*, 2126–2132. [CrossRef] [PubMed]
26. Chen, V.B.; Arendall, W.B., III; Headd, J.J.; Keedy, D.A.; Immormino, R.M.; Kapral, G.J.; Murray, L.W.; Richardson, J.S.; Richardson, D.C. MolProbity: All-atom structure validation for macromolecular crystallography. *Acta Crystallogr. D Biol. Crystallogr.* **2010**, *66*, 12–21. [CrossRef]
27. DeLano, W.L.; Lam, J.W. PyMOL: A communications tool for computational models. *Abstr. Pap. Am. Chem. Soc.* **2005**, *230*, U1371–U1372.
28. Vuoristo, K.S.; Mars, A.E.; van Loon, S.; Orsi, E.; Eggink, G.; Sanders, J.P.; Weusthuis, R.A. Heterologous expression of Mus musculus immunoresponsive gene 1 (irg1) in Escherichia coli results in itaconate production. *Front Microbiol.* **2015**, *6*, 849. [CrossRef] [PubMed]
29. Ashkenazy, H.; Erez, E.; Martz, E.; Pupko, T.; Ben-Tal, N. ConSurf 2010: Calculating evolutionary conservation in sequence and structure of proteins and nucleic acids. *Nucleic Acids Res.* **2010**, *38*, W529–W533. [CrossRef]
30. Lohkamp, B.; Bauerle, B.; Rieger, P.G.; Schneider, G. Three-dimensional structure of iminodisuccinate epimerase defines the fold of the MmgE/PrpD protein family. *J. Mol. Biol.* **2006**, *362*, 555–566. [CrossRef] [PubMed]